Multiplexed stimuli-responsive molecules for high-security anti-counterfeiting applications

ARTICLE

Multiplexed stimuli-responsive molecules for high-security anti-counterfeiting applications

Received 00th January 20xx,
Accepted 00th January 20xx

DOI: 10.1039/x0xx00000x

Hongyan Xia, [a,b] Tommy Loan, [b] Mithun Santra, [b] Kang Xie [*a] and Mark Bradley [*b]

In the context of society's increasing reliance on information, improving the level of data security is a key task but also a formidable challenge. As such it is necessary and urgent to develop advanced technologies for high-security information encryption. Herein, we efficiently synthesized a novel indole dimer (ID) which displayed multiple stimuli-driven chromotropic capabilities. When triggered by stimuli, the color of the compound changes rapidly, accompanied by reversible changes in fluorescence. Interestingly, the color changes of the indole dimer were orthogonal to those of the traditionally utilized stimuli-responsive spiropyran (SP). In combination, this allowed the preparation of invisible inks for printing, with security of information encrypted based on their diametrically opposed response to thermal and acid/base stimulation. The newly synthesized stimuli-responsive ID and the novel strategy of its application, in combination with the traditional stimuli-responsive SP provide a new direction in allowing high-level information security against forgery.

Introduction

With the increasing development of an information-based society, the problems surrounding information security have become increasingly serious and have gained extensive attentions, not only within the global economy, but also within our personal day-to-day lives.[1-5] Many previous activities have focused on simple, single-stage encryption and anti-counterfeiting technologies, such as watermarks, holograms and taggants. However, these are relatively inefficient as they can be easily deciphered or copied. Thus, constant efforts are exerted to develop higher level encryption/decryption technologies to protect information or prevent counterfeiting.[6-11] One efficient approach to enhance information protection is the utilization of multiplexed and smart stimuli-responsive materials which can be dynamically switched between different states during the "read" process.[12-15] Considerable advances in stimuli-responsive materials for information encryption have been made over the past few decades,[16-19] and for instance, Le *et al* realized programmable information protection based on stimuli-responsive hydrogels whose fluorescence is switched off by the external stimuli of metal ions that triggers the activity of an embedded enzyme.[20] Gao *et al* achieved multidimensional and multistage data encryption through the synergic responsiveness of fluorescence and shape triggered by a combination of the stimuli of light and heat.[21]

Among different kinds of stimuli-responsive materials for information security, chromic materials with reversible color switching in response to external stimuli are one of the most fascinating and widespread because changes in color are highly noticeable and can be discerned directly visually without the need for costly instrumentation.[22-26] Stimuli-responsive chromic materials have been studied as smart materials and applied widely in areas such as camouflage and anticounterfeiting displays,[27,28] rewritable paper,[29,30] security inks[31,32] and so on, with changes in color conveying more useful information to the observer, because the human visual perception is much more effective than other senses.[33,34] Traditional and commonly reported stimuli-responsive, chromic materials are diarylethenes,[35-37] spiropyrans,[38-40] fulgides,[41-43] azobenzenes[44,45] and their derivatives.[46] However, the existing molecules have long been developed, and as such their properties are well known and are familiar to counterfeiters, such that they are now readily forged and "cracked" when applied in the field of information encryption.[47] Progress in related fields has been relatively slow due to the lack of high-performance smart materials, and the fabrication of stimuli-responsive chromogenic systems is also critical yet challenging.[48] Current efforts in this area focus on designing and exploiting new stimuli-responsive chromic molecules and extending their applications.[49] At the same time, construction of multi-mode and high-level stimuli-responsive systems with good confidential encryption abilities is an essential requirement for advanced information protection as well.[50] Thus Zhang *et al* reported a multiple encryption supramolecular gel which self-assembled using three different chromogens, giving rise to pink, purple and yellow colors when subjected to

[a] *H. Xia, K. Xie*
State Key Laboratory of Precision Electronic Manufacturing Technology and Equipment, School of Electromechanical Engineering
Guangdong University of Technology
Guangzhou, Guangdong 510006, China
Email: kangxie@gdut.edu.cnAddress here.
[b] *H. Xia, L. Hu, M. Santra, T. Loan, M. Bradley*
EaStCHEM School of Chemistry
University of Edinburgh
Edinburgh EH9 3FJ, United Kingdom
Email: mark.bradley@ed.ac.uk

different stimuli, the encoded information only be readable by treating with all three stimulus "keys", endowing the system with a high-level encryption security.[51]

Herein we designed and synthesized a new type of stimuli-responsive chemical entity based on a novel indole dimer (ID) which showed good stability and rapid color switching rates in response to acid/base. Protonation and deprotonation naturally leads to changes in their electron distribution, resulting in a series of changes in their optical properties.[52-56] ID showed excellent acid/base responsive chromism reversibly due to the basicity of the indole unit when attached to a conjugated alkene, which was readily protonated/deprotonated under acidic/basic conditions (Scheme 1). The molecular conformation and frontier molecular orbitals (through the density functional theory calculations) of the ID were significantly affected by the presence of acid/base and as expected, the optical behavior was strongly influenced by the charge delocalization and variations in the charge density around the indole ring. Here, the ID was used as an invisible ink in combination with the spiropyran (one of the most versatile classes of stimuli-responsive chromic materials) which will change color and structure under external stimuli between spiropyran (SP) form, merocyanine (MC) form and protonated merocyanine ($MC\text{-}H^+$) form [57,58]. The ink composed of these two compounds is suitable for inkjet printing and can realize the high-level information encryption by taking advantage of their responsiveness to heat and acid/base orthogonality (Scheme 1).[59,60] The encrypted information could be reversibly switched between "Encrypted", "Fake" or "Authentic" and could also be "protected" from being "leaked" to the unauthorized personnel. There exist numerous unique advantages of this smart chromic anti-counterfeiting system compared to others: (i) ID is a new compound and being used in "anti-counterfeiting" for the first time, so it's more difficult to be forged and duplicated by counterfeiters; (ii) The information security is enhanced significantly through dual usage of ID with SP due to their orthogonal responsiveness to the same stimuli; (iii) Facile ink preparation and inkjet printing pave a new avenue for the generation of complicated and high-level anti-counterfeiting words/patterns at low cost, yet with high resolution and large scale potential. This multi-responsive and multi-mode encryption strategy endows good confidential encryption abilities for a new generation of high-security information encryption platforms.

Scheme 1. The chemical structures and color transformations of ID (indole dimer) and SP (spiropyran) under different external stimuli, and their combination as an ink for high-level information encryption.

Experimental Section

Materials

2-(3′,3′-Dimethyl-6-nitrospiro[chromene-2,2′-indolin]-1′-yl)ethanol (spiropyran), Trifluoroacetic acid (TFA) and Triethylamine (TEA) were purchased from Fluorochem Ltd. 2-phenylindole, CH_3COCl, CH_3COOH, sodium bicarbonate, magnesium sulphate, Cs_2CO_3 and bromoethane were all obtained from Sigma-Aldrich. All reagents and solvents were of analytical grade and used as received without any further treatment.

Synthesis

(1) synthesis of the1-ethyl-2phenylindole: To a solution of 2-phenylindole (2.0 g, 10 mmol) in anhydrous acetonitrile, was added Cs_2CO_3 (6.5g, 20 mmol) and bromoethane (1.47 ml, 20 mmol), then was heated at 70 °C for 6h. The mixture was cooled to room temperature, diluted with water, extracted with ethyl acetate and dried with $MgSO_4$. The collected organic fractions were concentrated in vacuo and the crude product was purified by column chromatography on silica gel (eluent = ethyl acetate /hexane (1:19)) to afford the desired product as a light-yellow solid (1.2 g). (2) synthesis of 3, 3'-Ethenylidenebis[1-ethyl-2-phenyl-1H-indole] (indole dimer, ID): To a solution of 1-ethyl-2-phenylindole (1.0 g, 4.52 mmol) in CH_3COOH (10 mL), CH_3COCl (321 µL, 4.52 mmol) was added slowly over 5 min. The reaction mixture was heated to 70 °C for 5 h before cooling to room temperature. Then the mixture was poured to water and neutralized by saturated sodium bicarbonate ($NaHCO_3$) solution, and then extracted using ethyl acetate (10ml) three times. The organic layer was washed with brine and dried over anhydrous $MgSO_4$. The solvent was removed in vacuo and subjected to flash column chromatography on silica gel (eluent = ethyl acetate /hexane (1:10)) to afford the desired product as a white solid (350 mg).

Theoretical calculation details

DFT calculations were performed using a Gaussian 09 program package. All structures were optimized at the TPSSh level of theory with the def2-SVP basis set. Binding energies were calculated using the counterpoise corrections method at the TPSSh/def2-TZVP level. TD-DFT (time-dependent density functional theory) calculations were performed at the TPSSh/def2-TZVP level, UV-Vis and electronic circular dichroism (ECD) spectrum plots were generated using the Multiwfn 3.8 program.

Preparation of information images

The information images were prepared by inkjet printing. The ID (concentration: 50mg/ml) and SP (concentration: 30mg/ml) dissolved in 1-Methyl-2-pyrrolidinone (NMP) and used as the visible inks for printing using a non-contact sciFLEXARRAYER S5 inkjet printing system (Scienion, Germany) equipped with a PDC 80 Piezo Dispense Capillary (Piezo Systems, Massachusetts, USA; 50 µm nozzle aperture). For simple "information" encryption, the "Cat" and "Rabbit" images were printed on paper substrates using two NMP solutions. For high-level information encryption, the two images were printed on the (same) paper substrate. The colorless ID NMP solution was first

printed on the paper to give the "Rabbit" pattern and then the colorless SP (NMP solution) was printed on the same substrate to give the "cat" pattern (See Figure 6).

Measurements

UV–vis absorbance spectra were measured using an UV/vis spectrophotometer (Agilent 8453). The fluorescence spectra of the solutions were determined on a spectrofluorophotometer (Shimadzu RF-6000) with a xenon lamp excitation light source with an interval of 1 nm and a scan speed of 6000 nm/min. All spectral measurements were obtained in a quartz sample cell (with a 1 cm path length) at room temperature. ^{1}H NMR spectra were recorded on a Bruker AVA500 spectrometer (500MHz) at 298 K in deuterated solvents ($CDCl_3$). Thermal gravimetric analysis (TGA) was carried out on a SDT Q600 V8.3 Build 101 thermal analyzer instrument under Argon atmosphere at a heating rate of 10 °C/min from 0 to 500 °C. Fourier transform infrared (FT-IR) spectra were obtained on a Nicolet 6700 FT-IR spectrometer. X-ray photoelectron spectra (XPS) were carried out with ESCALAB Xi+ (Thermo Scientific).

Results and discussion

Synthesis and characterization

The smart stimuli-responsive indole dimer (ID) was synthesized via two synthetic steps as shown in Figure 1 (see Experimental Section and Figure S1 for the synthesis process and ^{1}H NMR characterization data).

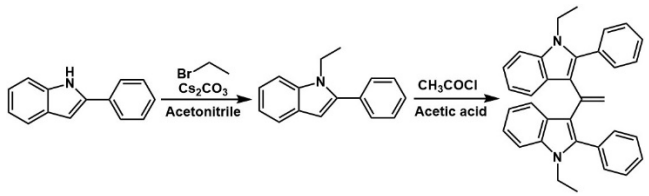

Figure 1. Synthetic route to the indole dimer (ID).

Dynamic thermogravimetric analysis (TGA) was carried out to investigate the thermal stability of ID (Figure S2) with the temperature onset of mass loss beginning around 270 °C, with an obvious weight loss of ID in the range between 274 °C to 385 °C. The temperature of rapid decomposition (T_{decomp}) was 363 °C, with a T_d of 280 °C (T_d, being the temperature at which 5% weight loss occurs and is often used to estimate the thermal stability of a material). The TGA results showed that ID was suitable for various applications, as it was thermally very robust below 270 °C.

Reversible acid/base responsive properties of the ID

Due to two indole groups and the conjugated alkene, the ID could reversibly be protonated/deprotonated upon treatment with acid and base, leading to associated changes in the absorption and fluorescence spectra. Figure 2a shows the spectral changes in the absorption spectrum of the ID upon the addition of protons (here using trifluoroacetic acid (TFA)), with the absorption peak at 313nm decreasing and the growth of a new absorption peak at 531nm. Indeed, a solution of the ID in CH_2Cl_2 was colorless, but when TFA was added, the color changes observed were from colorless to pale magenta and finally plateauing to deep magenta (Figure 2b, c and d). The molar extinction coefficient changed from 1.65 x 10^4 (313 nm) to 3.42 x 10^4 (531nm) L mol^{-1} cm^{-1} with an isosbestic point at approximately 350 nm, demonstrating the formation of new species. We suggested that the ID was protonated upon adding acid.

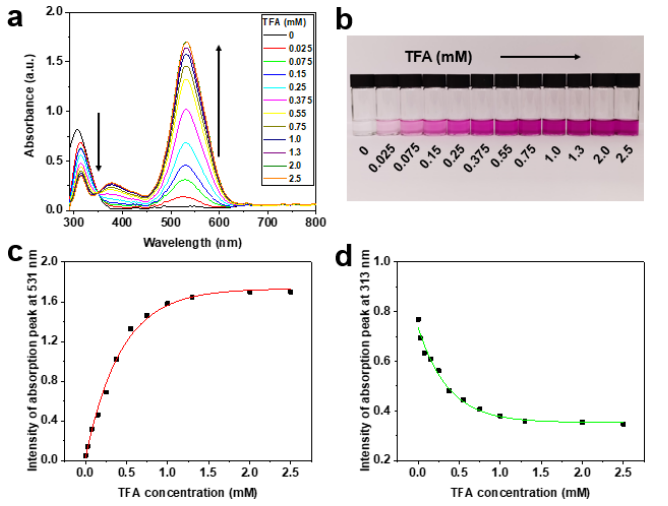

Figure 2. (a) UV-Vis absorption changes and (b) Images of the ID in CH_2Cl_2 (0.05mM) upon the addition of different concentrations of TFA (from 0 to 2.5 mM). Intensity changes in absorption peaks at (c) 531 nm and (d) 313 nm of the ID with different concentrations of TFA.

The protonated ID (ID-H$^+$) underwent rapid deprotonation upon treatment with the base (triethylamine, TEA), with the colored solution recovering to the original absorption spectra with increasing the amounts of base (Figure S3). The intensity variation in the absorption peaks at 313 nm and 531 nm were robust over 65 consecutive cycles without obvious attenuation, indicating the excellent reversibility of the acid/base responsiveness of the reporter (Figure 3).

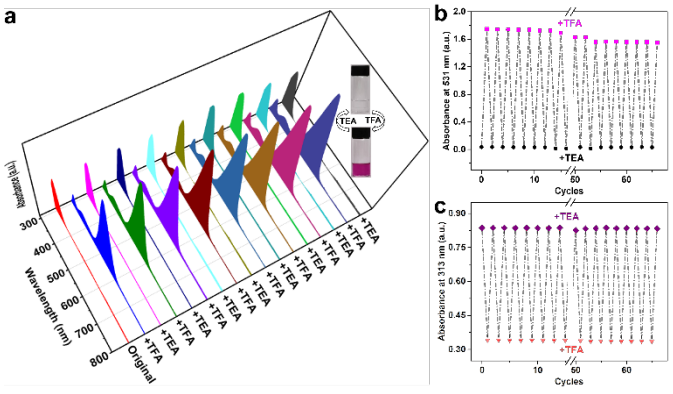

Figure 3. Reversible UV-Vis absorption spectra changes of the ID in CH_2Cl_2 (0.05 mM) following the treatment with TFA and TEA. Inset: Images of the ID in CH_2Cl_2 after adding TFA and TEA. Intensity changes in the absorption peak at (b) 531nm and (c) 313nm following reversible treatment with TFA and TEA over 65 cycles.

When acid was added to the ID solution, the fluorescent emission at 405 nm decreased gradually with a new emission peak at 671nm that intensified with increasing amounts of TFA (see Figure 4). When the solution was treated with base, the

large shift (266 nm) in the fluorescence was recovered, demonstrating the significant fluorescence switching properties of the ID under protonation-deprotonation stimuli. Through plotting the fluorescence peak intensity at 405 nm and 671 nm as a function of TFA concentration, the relationship between emission intensities and TFA content were obtained (Figure 4b and 4e). Fluorescent titration experiments confirmed the binding number (n) of ID with H^+ and the binding association constant (K_{ass}). Thus as shown in Figure 4f, a good linear relationship between the lg[H^+] and the lg[(F_{max}-F)/(F-F_{min})] was obtained, giving a binding number for ID to be 1.07, which showed that ID bind with H^+ in a ratio of 1:1 (one molecule binds with one proton). The lgK_{ass} value was found to be 5.34.[61,62] The response time, estimated from the time-course of the fluorescence quenching curve of the ID solution, was as short as 0.92s (Figure 4c).

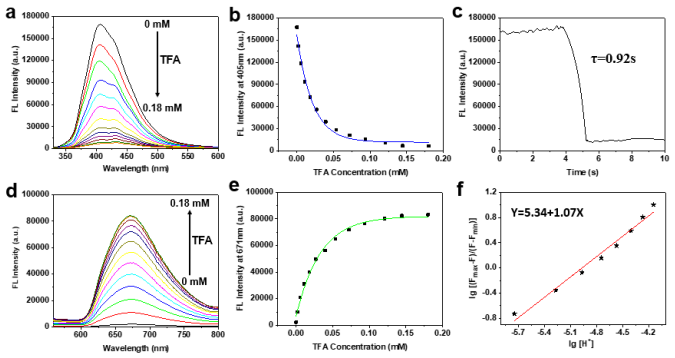

Figure 4. Fluorescence spectral changes of the ID in CH_2Cl_2 (0.0035 mM) with different concentrations of TFA (0 to 0.18 mM) with excitation at (a) 320nm and (d) 530nm. Intensity changes of fluorescence peak at (b) 405 nm and (e) 671 nm of the ID in CH_2Cl_2 with different concentrations of TFA. (c) Time-course of fluorescence quenching of the ID in CH_2Cl_2 upon the addition of TFA (0.144 mM), the intensity was monitored at 405 nm with an excitation wavelength of 320 nm. (f) A plot of emission intensity at 405 nm *vers* hydrogen ion concentration with ID in CH_2Cl_2 under the excitation at 320 nm.

It was observed that upon addition of acid, the alkene resonance (around 5.2 ppm, Figure 5) disappeared, with the original methylene group becoming a methyl group upon protonation with a new chemical shift (ascribed to the methyl group, around 2.3 ppm) appearing. Also, the original (equivalent) two ethyl groups became distinguishable, the structure giving rise to two different electronic environments, presumably either due to the non-symmetrical form of the cation (as drawn in Figure 5), or the isomeric (E) cationic form. Other changes in the NMR spectra were consummate with this protonated form.

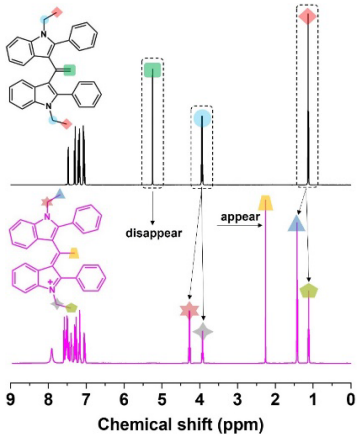

Figure 5. ^{1}H NMR spectra of the ID before (black) and after (purple) the addition of 2.5 mM TFA ($CDCl_3$, 500MHz at 298K).

Fourier transform infrared (FT-IR) and X-ray photoelectron spectra (XPS) spectra were also introduced to investigate the structure change of ID before and after protonation. As shown in Figure S4, the C-H bond vibration peak (879 cm^{-1}) of -C=CH_2 on the structure of ID is very strong, while the peak intensity of C-H bond of -C=CH_2 decreases significantly after protonation due to the reduction content of C=C double bonds. The high-resolution XPS N 1s spectra of ID was peak-differentiated to one type of nitrogen at 400.1eV which ascribed to the N-C bond, while the N 1s of ID-H^+ were deconvoluted into two peaks at 400.1eV and 401.1eV, which indicated the presence of N-C (400.1 eV) and N=C (401.1 eV) bonds (Figure S5). These results implied the structure change of ID before and after protonation which agreed well with the NMR results.

Density function theoretical calculations

Density functional theory (DFT) calculations were carried out for the ID before and after protonation by the Gaussian 09 program to analyze its frontier molecular orbitals and electronic properties.[63-65] The optimized molecular conformations of the ID before and after protonation are shown in Figure S6. It was found that the conformation of the ID before and after protonation changed significantly. The dihedral angle between the phenyl and the indole unit plane of ID-H^+ reduced upon protonation side due to the steric hindrance compared with the ID which adopted a more twisted conformation. As shown in **Figure 6,** there is a large difference in electron cloud distribution of the frontier molecular orbitals of the ID before and after protonation. The calculated highest occupied molecular orbitals (HOMO) and the lowest unoccupied molecular orbitals (LUMO) energy levels were -5.28 and -1.16 eV for the ID, as well as -2.62 and -0.95eV for ID-H^+. The energy gap Eg was 4.12 eV for the ID, and 1.67eV for the ID-H^+, agreeing well with optical gap obtained from UV/Vis absorption profiles for the ID and the ID-H^+. Thus protonation reduced the HOMO-LUMO gap of the ID, with the decrease in energy upon protonation supporting our experimental results of an absorption spectral red-shift. The DFT calculations gave the simulated absorption spectra which also matched well with the experimental data (Figure S7). The change in the electron cloud density of the ID molecule before and after protonation influences its frontier molecular orbitals,

leading to the absorption (from 313 nm to 531 nm) and fluorescence (from 405 nm to 671 nm) bathochromic-shift.

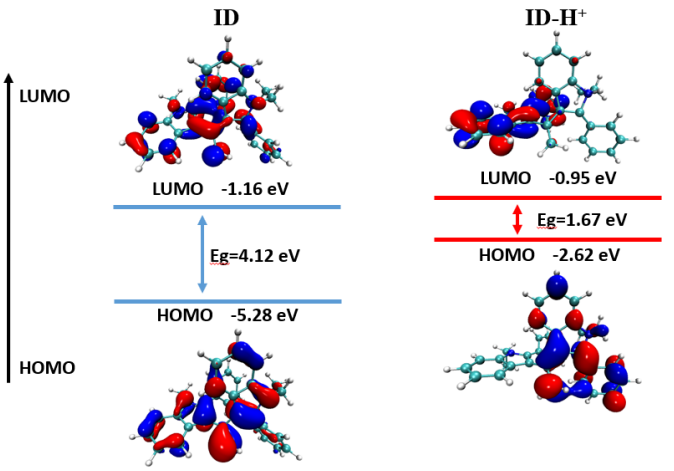

Figure 6. The energy level diagrams and molecular frontier orbital contributions of the ID and the ID-H+.

High-security information encryption

On the basis of the stimuli-responsive features of the ID, its application as an invisible security ink was explored. "Information Images" were printed with the transparent ID solution ink through inkjet printing. As shown in Figure 7a, after printing, the "Rabbit" image was invisible, and the information was in the encrypted state. Upon heating (80 ℃, 10 s), the encrypted information was still in the encrypted state due to the robust thermal stability of the ID. When stimulated with acid vapor, the "Rabbit" image appeared, returning the decrypted information (due to protonation which was colored). The decrypted information was rapidly re-hidden by treatment with base vapor due to the deprotonation, a process that could be repeated many times (see Video S1).

Following the same process as the above, the image of a "Cat" was printed using the invisible SP ink. After printing, the image was also invisible, but upon heating (80 ℃, 10s), the encrypted information was decrypted due to the structural transformation of SP to MC which is colored. When the image was treated with acid vapor, the MC was protonated to MC-H+ which is almost colorless, and thus the image of the "Cat" disappeared (information encrypted). Subsequently, when the image was treated with base vapor, the encrypted information was "decrypted" again because the MC-H+ transferred to the colored MC form, allowing the "Cat" to be observed (Figure 7b). The corresponding absorption spectra and color changes for the compounds SP, MC and MC-H+ on the glass slide under external stimuli are displayed in Figure S8, consistent with the color changes of the "Cat" on the paper. Similarly, the encryption-decryption process based on the SP could be repeated many times (shown in the Video S2).

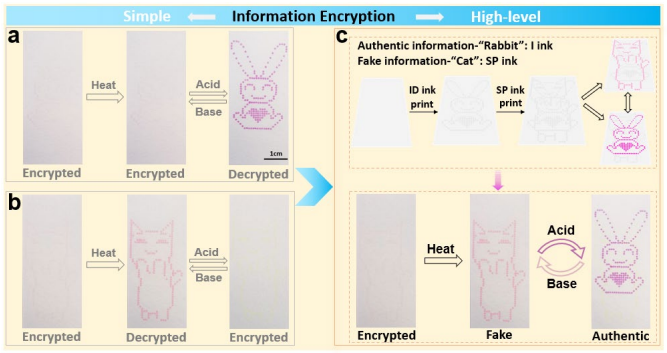

Figure 7. (a) The switch-on/off of images of the printed "Rabbit" by the ID ink under different external stimuli. (b) The switch-on/off of images of the printed "Cat" by the SP ink under different external stimuli. (c) Printing of the "Rabbit" and "Cat" images by the ID and SP inks and the switch between different visible images under external stimuli (upper). The switch of images from nothing (invisible), and the switch of the "Cat" and "Rabbit" images under external stimuli (lower).

Comparing the above two processes, we were intrigued to find that the ID and the SP had exactly the opposite responses to heat and acid/base treatments. The ID had good thermal stability and was colorless before and after heating, while the SP changed from colorless to the colored form after heating. The ID changed from colorless to colored upon exposure to acid and the color changed back to colorless upon exposure to base. But the spiropyran changed from colored MC form to colorless SP form upon exposure to acid and changed back to the colored MC upon exposure to base (the process is opposite to that of the ID). Thus a new strategy for high-level information encryption by combining them together was proposed. Thus as shown in Figure 7c, on the same substrate, the authentic image "Rabbit" was printed using the ID ink and the fake image "Cat" was printed using the SP ink. All the images were invisible upon printing and the information was in the "locked" state. Upon heating (80 ℃, 10 s), a bright "Cat" appeared due to the transformation of the SP to the colored MC form, with the ID remaining in the colorless state, so the "Rabbit" was invisible at this time, so the presented information was "fake". Subsequently, upon exposure to acid vapor, the "Cat" disappeared and the vivid magenta "Rabbit" could be clearly seen due to the transformation of the ID to the ID-H+ and the MC to MC-H+, giving the "Rabbit" authentic image. After we generated the correct information, we could also treat the authentic information with base vapor to return it to the "fake" form, improving the information protection capabilities greatly. The above process also possessed very good reversibility as shown in Video S3. This kind of combination could also survive repeated cycles of "encryption-decryption". The initial invisible feature of this system made the confidential information well-hidden and unrecognizable, and the existence of the fake information would also confuse the counterfeiters further. The readers couldn't also recognize which was the "true" information without any additional knowledge, thus significantly improved the complexity and concealment of the encrypted information, achieving high-level security. This strategy provides a new choice for more secure information encryption, such that only the trained and authorized

information receiver, who knows the correct algorithm, was able to access the confidential information.

Conclusions

In summary, a novel type of smart compound ID was synthesized and exhibited outstanding stimuli-responsive chromic properties due to protonation and deprotonation of the indole unit, the conformations and frontier molecular orbital can be also significantly affected by the external stimuli. Taking advantage of its unique responsiveness, its application as the invisible security ink in the field of anti-counterfeiting was first explored. ID can mimic proton transfer processes in nature at the molecular level, it also changes the structure, color and emission through proton transfer under external stimuli, which brings hope for the subsequent anti-counterfeiting application in natural and biological systems. Most interestingly, the response of the ID to heat and acid/base was orthogonal to the traditionally utilized stimuli-responsive compound SP and by applying these compounds together in one system after printing, different patterns appeared under different external stimuli, allowing high-level and complicated information encryption and decryption to be realized. The new compound we fabricated and the synergistic usage strategy of these two smart materials, with opposite responses to the same stimulus in this work, opens up a new insight for the design and manufacture of extra-safety in information encryption technologies, and has broad and promising application prospects in the information anti-counterfeiting fields.

Author Contributions

H. Xia designed the experiments and wrote the paper. L. Hu prepared the samples. M. Santra carried out the tests. T. Loan discussed the results. K. Xie and M. Bradley contributed to write and edit the paper.

Conflicts of interest

There are no conflicts to declare.

Acknowledgements

This project has received funding from the European Union's Horizon 2020 research and innovation program under the Marie Skłodowska-Curie grant agreement (No. 896348), the National Natural Science Foundation of Guangdong, China (No. 2021A1515012348), the Science and Technology Planning Project of Guangzhou (No. 202102020782), the Leading Talents of Guangdong Province Program, and the National Natural Science Foundation of China (No. 11874126).

References

1 Z. Zeng, B. Huang, X. Wang, L. Lu, Q. Lu, M. Sun, T. Wu, T. Ma, Y. Xu, S. Wang, Y. Du, C. H. Yan, *Adv. Mater.*, 2020, **32**, e2004506.
2 C. N. Zhu, T. Bai, H. Wang, J. Ling, F. Huang, W. Hong, Q. Zheng, Z. L. Wu, *Adv. Mater.*, 2021, **33**, 2102023.
3 J. Tan, Q. Li, S. Meng, Y, Li, J. Yang, Y. Ye, Z. Tang, S. Qu, X. Ren, *Adv. Mater.*, 2021, **33**, 2006781.
4 R. Arppe, T. J. Sørensen, Nat. Rev. Chem. 2017, 1, 0031.Y. Wen, Q. Zhou, X. Su, D. Hu, M. Xu, W. Feng, F. Li, *ACS Appl. Mater. Interfaces*, 2022, **14**, 11681-11689.
5 Y. Wu, W. Wu, *Adv. Optical Mater.* **2021**, *9*, 2100281.
6 W. Yao, Q. Tian, W. Wu, *Adv. Optical Mater.* **2019**, *7*, 1801171.
7 M. Li, D. Yang, X. Huang, H. Zhang, Y. Zhao, B. Yin, Q. Pan, J. Kang, N. Zheng, X. Liu, J. Qiu, Z. Yang, G. Dong, *Adv. Mater.*, 2022, **34**, 2201413.
8 W. Ren, G. Lin, C. Clarke, J. Zhou, D. Jin, *Adv. Mater.,* 2020, **32**, 1901430.
9 Y. Zhang, X. Le, Y. Jian, W. Lu, J. Zhang, T. Chen, *Adv. Funct. Mater.,* 2019, **29**, 190551.
10 A. M. Kaczmarek, Y. Liu, C. Wang, B. Laforce, L. Vincze, P. V. D. Voort, K. V. Hecke, R. V. Deun, *Adv. Funct. Mater.,* 2017, **27**, 1700258.
11 P. Feng, X. Yang, X. Feng, G. Zhao, X. Li, J. Cao, Y. Tang, C. Yan, *ACS Nano,* 2021, **15**, 6266-6275.
12 D. Chen, C. Cui, N. Tong, H. Zhou, X. Wang, R. Wang, *ACS Appl. Mater.* Interfaces 2019, **11**, 1480-1486.
13 Z. Song, T. Lin, L. Lin, S. Lin, F. Fu, X. Wang, L. Guo, *Angew. Chem. Int. Ed.,* 2016, **55**, 2773– 2777.
14 X. Li, Y. Xie, B. Song, H. Zhang, H. Chen, H. Cai, W. Liu, Y. Tang, *Angew. Chem. Int. Ed.,* 2017, **56**, 2689-2693.
15 K. Jiang, L. Zhang, J. Lu, C. Xu, C. Cai, H. Lin, *Angew. Chem. Int. Ed.,* 2016, **55**, 7231– 7235.
16 J. Li, X. Huang, X. Zhao, L. J. Chen, X. P. Yan. *Angew. Chem. Int. Ed,.* 2021, **60**, 2398-2405.
17 X. Liu, Y. Wang, X. Li, Z. Yi, R. Deng, L. Liang, X. Xie, D. T. B. Loong, S. Song, D. Fan, *Nat. Commun.,* 2017, **8**, 899.
18 J. Deng, H. Wu, W. Xie, H. Jia, Z. Xia, H. Wang, *ACS Appl. Mater. Interfaces* 2021, **13**, 39967-39975.
19 J. Wang, B. Jin, N. Wang, T. Peng, X. Li, Y. Luo, S. Wang, *Macromolecules,* 2017, **50**, 4629-4638.
20 X. Le, H. Shang, H. Yan, J. Zhang, W. Lu, M. Liu, L. Wang, G. Lu, Q. Xue, T. Chen, *Angew. Chem. Int. Ed.,* 2021, **60**, 3640–3646.
21 [J. Gao, M. Tian, Y. He, H. Yi, J. Guo, *Adv. Funct. Mater.,* 2022, **32**, 2107145.
22 G. Lee, M. Kong, D. Park, J. Park, U. Jeong, *Adv. Mater.,* 2020, **32**, 1907477.
23 D. Li, Z. Feng, Y. Han, C. Chen, Q. Zhang, Y. Tian, *Adv. Sci.,* 2022, **9**, 2104790.
24 G. Xi, L. Sheng, J. Du, J. Zhang, M. Li, H. Wang, Y. Ma, S. X. Zhang, Nat. *Commun.,* 2018, **9**, 4819.
25 T. Yuan, M. Vazquez, A. N. Goldner, Y. Xu, R. Contrucci, M. A. Firestone, M. A. Olson, L. Fang, *Adv. Funct. Mater.,* 2016, **26**, 8604-8612.
26 T. Zhang, L. Sheng, J. Liu, L. Ju, J. Li, Z. Du, W. Zhang, M. Li, S. X. Zhang, *Adv. Funct. Mater.,* 2018, **28**, 1705532.
27 A. Abdollahi, H. Roghani-Mamaqani, B. Razavi, M. Salami-Kalajahi, *ACS Nano,* 2020, **14**, 14417-14492.
28 Y. Wang, Y. Zhang, S. X. Zhang, *Acc. Chem. Res.,* 2021, **54**, 2216-2226.
29 L. Mao, Z. Wang, Y. Duan, C. Xiong, C. He, X. Deng, Y. Zheng, D. Wang, *ACS Nano,* 2021, **15**, 10384-10392.
30 W. Wang, N. Xie, L. He, Y. Yin, Nat. *Commun.,* 2014, **5**, 5459.
31 H. Zhao, X. Qin, L. Zhao, S. Dong, L. Gu, W. Sun, D. Wang, Y. Zheng, *ACS Appl. Mater. Interfaces* 2020, **12**, 8952-8960.
32 Q. Zhou, X. Qiu, X. Su, Q. Liu, Y. Wen, M. Xu, *Small,* 2021, **17**, 2100377.
33 W. Tian, J. Zhang, J. Yu, J. Wu, J. Zhang, J. He, F. Wang, *Adv. Funct. Mater.,* 2018, **28**, 1703548.

34 L. R. Gregory, *Nature,* 1965, **207**, 16.
35 Z. Zhang, W. Wang, P. Jin, J. Xue, L. Sun, J. Huang, J. Zhang, H. Tian, *Nat. Commun.,* 2019, **10**, 4232.
36 S. Lin, K. G. Gutierrez-Cuevas, X. Zhang, J. Guo, Q. Li, *Adv. Funct. Mater.,* 2021, **31**, 2007957.
37 W. Jeong, M. I. Khazi, D. Park, Y. Jung, J. M. Kim, *Adv. Funct. Mater.,* 2016, **26**, 5230-5238.
38 H. Ju, C. N. Zhu, H. Wang, Z. A. Page, Z. L. Wu, J. L. Sessler, F. Huang, *Adv. Mater.,* 2022, **34**, 2108163.
39 Y. Yang, Y. Li, Y. Chen, Z. Wang, Z. He, J. He, H. Zhao, *ACS Appl. Mater. Interfaces,* 2022, **14**, 21330−21339.
40 Y. Shi, J. Han, X. Jin, W. Miao, Y. Zhang, P. Duan, *Adv. Sci.,* 2022, **9**, 2201565.
41 G. Tomasello, M. J. Bearpark, M. A. Robb, G. Orlandi, M. Garavelli, *Angew. Chem. Int. Ed.,* 2010, 49, 2913−2916.
42 Y. Yokoyama, *Chem. Rev.* 2000, **100**, 1717−1740.
43 S. Padgaonkar, C. T. Eckdahl, J. K. Sowa, R. Lopez-Arteaga, D. E. Westmoreland, E. F. Woods, S. Irgen-Gioro, B. Nagasing, T. Seideman, M. C. Hersam, J. A. Kalow, E. A. Weiss, *Nano Lett.,* 2021, **21**, 854−860.
44 Y. Liu, S. Liang, C. Yuan, A. Best, M. Kappl, K. Koynov, H. Butt, S. Wu, *Adv. Funct. Mater.,* 2021, **31**, 2103908.
45 C. Zhai, G. Fang, W. Liu, T. Wu, L. Miao, L. Zhang, J. Ma, Y. Zhang, C. Zong, S. Zhang, C. Lu, *ACS Appl. Mater., Interfaces* 2021, **13**, 42024-42034.
46 S. Tang, J. An, F. Song, M. Lv, K. Han, X. Peng, *ACS Appl. Mater. Interfaces*, 2021, **13**, 51414-51425.
47 K. Jiang, Y. Wang, C. Cai, H. Lin, *Adv. Mater.*, 2018, 30, 1800783.
48 Q. Qi, C. Li, X. Liu, S. Jiang, Z. Xu, R. Lee, M. Zhu, B. Xu, W. Tian, *J. Am. Chem. Soc.,* 2017, **139**, 16036−16039.
49 Y. Ma, Y. Yu, P. She, J. Lu, S. Liu, W. Huang, Q. Zhao, *Sci. Adv.,* 2020, **6**, eaaz2386.
50 Z. Du, T. Zhang, H. Gai, L. Sheng, Y. Guan, X. Wang, T. Qin, M. Li, S. Wang, Y. Zhang, H. Nie, S. X. Zhang, *Adv. Sci.,* 2022, **9**, 2103309.
51 H. Zhang, Q. Li, Y. Yang, X. Ji, J. L. Sessler, *J. Am. Chem. Soc.,* 2021, **143**, 18635−18642.
52 J. B. Arockiam, S. Ayyanar, Sens. *Actuator B Chem.,* 2017, **242**, 535-544.
53 S. Cui, B. Wang, Y. Teng, Z. Wan, Y. Zan, L. Chen, Y. Li, X. Yan, *Sens. Actuator B Chem.*, 2021, **344**, 130120.
54 X. Zhang, J. Wang, H. Liu, F. Yu, T. Wang, X. Huang, H. Hao, *Dyes Pigm.,* 2022, **197**, 109903.
55 H. Liang, B. Hua, F. Xu, L. Gan, L. Shao, F. Huang, *J. Am. Chem. Soc.,* 2020, **142**, 19772−19778.
56 Y. Li, X. Wang, L. Zhang, L. Liu, Q. Wang, H. Lu, X. Zhao, *Mater. Chem. Front*., 2020, **4**, 3378-3383.
57 R. Klajn, Chem. Soc. Rev. 2014, **43**, 148-184.
58 L. Kortekaas, W. R. Browne, *Chem. Soc. Rev.,* 2019, **48**, 3406-3424.
59 A. Julià-López, J. Hernando, D. Ruiz-Molina, P. Gonzµlez-Monje, J. Sedó, *C. Roscini, Angew. Chem.,* 2016, **128**, 15268–15272.
60 T. R. Evans, A. F. Toth, P. A. Leermakers, *J. Am. Chem., Soc.* 1967, **89**, 5060 –5061.
61 F. Zhao, T. Sun, Y. Wang, Y. Zhan, W. Yang, *Dyes Pigm.,* 2021, **196**, 109763.
62 Y. Zhang, *Dyes Pigm.,* 2020, 173, 108002.
63 Y. Xu, C. Li, Z. Li, Q. Wang, X. Cai, J. Wei, Y. Wang, *Angew. Chem. Int. Ed.,* 2020, **59**, 17442 –17446.
64 T. D. Spivey, A. Holewinski, *J. Am. Chem. Soc.,* 2021, **143**, 11897–11902.
65 X. Ni, H. Li, F. Liu, *J. Brédas, Mater. Horiz.,* 2022, **9**, 88-98.